Blood flow coordinates collective endothelial cell migration during vascular plexus formation and promotes angiogenic sprout regression via *vegfr3/flt4*

Yan Chen[1], Zhen Jiang[2, 3], Katherine H. Fisher [4], Hyejeong R. Kim [4], Paul C. Evans[1]* and Robert N. Wilkinson[5]*

1 Department of Infection, Immunity and Cardiovascular Disease, University of Sheffield, UK
2 Max Planck Institute for Heart and Lung Research, Department of Developmental Genetics, Bad Nauheim 61231, Germany.
3 German Centre for Cardiovascular Research (DZHK), Partner Site Rhine-Main, Bad Nauheim 61231, Germany.
4 Department of Biomedical Science, University of Sheffield, UK
5 School of Life Sciences, Medical School, University of Nottingham, UK

*Equal contribution

Author for correspondence
Robert Wilkinson
rob.wilkinson@nottingham.ac.uk
Phone: +44 115 823 1429

Abstract

Nascent vascular networks adapt to the increasing metabolic demands of growing tissues by expanding via angiogenesis. As vascular networks expand, blood vessels remodel, progressively refining vascular connectivity to generate a more haemodynamically efficient network. This process is driven by interplay between endothelial cell (EC) signalling and blood flow. While much is known about angiogenesis, considerably less is understood of the mechanisms underlying vessel remodelling by blood flow. Here we employ the zebrafish sub-intestinal venous plexus (SIVP) to characterise the mechanisms underlying blood flow-dependent remodelling. Using live imaging to track ECs we show that blood flow controls SIVP remodelling by coordinating collective migration of ECs within the developing plexus. Blood flow opposes continuous ventral EC migration within the SIVP and is required for regression of angiogenic sprouts to support plexus growth. Sprout regression occurs by coordinated polarisation and migration of ECs from non-perfused leading sprouts, which migrate in opposition to blood flow and incorporate into the SIV. Sprout regression is compatible with low blood flow and is dependent upon *vegfr3/flt4* function under these conditions. Blood flow limits expansive venous remodelling promoted by *vegfr3/flt4*. Collectively, these studies reveal how blood flow sculpts a developing vascular plexus by coordinating EC migration and balancing vascular remodelling via *vegfr3/flt4*.

Introduction

During development, all cells must obtain nutrients and excrete waste by-products at stages when organs which will eventually perform these roles have not yet formed. Therefore, developing vascular networks which perform metabolic exchange at these stages must adapt rapidly to meet the changing metabolic demands of growing tissues. As vascular networks grow, they must maximise efficiency of metabolic exchange while minimising resistance to blood delivery, thus mechanisms which promote haemodynamic efficiency have been selected throughout evolution (Campinho et al., 2020). Production of new vessels by angiogenic sprouting must be balanced with progressive network refinement by remodelling to maintain haemodynamic efficiency within a developing vascular network. This occurs either by fusion or regression of angiogenic sprouts to form tubular vessels, or by pruning redundant blood vessels (Ribatti and Crivellato, 2012). Endothelial cells (ECs) line the inner surface of blood vessels. Vascular remodelling is driven by dynamic responses of ECs to changes in their local environment (Udan et al., 2013). Most blood vessels develop from existing patent vessels with stable blood flow and while much is known about sprouting angiogenesis, the understanding of mechanisms which govern vascular remodelling and how blood flow influences them remains incomplete. For example, it is unclear whether vascular regression is induced by active signalling pathways, withdrawal of survival factors, or a combination of both, and whether this is coordinated via distinct mechanisms in different vascular beds (Korn and Augustin, 2015).

The zebrafish sub-intestinal venous plexus (SIVP) is a vascular network which forms bilaterally in the embryo and is structurally similar to the mammalian vitelline veins which connect the embryo with extraembryonic circulation in the yolk sac (Goi and Childs, 2016). Due to its developmental plasticity the SIVP has emerged as a powerful model to characterise cellular mechanisms underlying vascular remodelling (Goi and Childs, 2016; Hen et al., 2015; Koenig et al., 2016; Lenard et al., 2015). The SIVP initially provides the developing embryo with nutrients from the yolk and later vascularises the digestive system in the larva (Isogai et al., 2001). The SIVP comprises the supra-intestinal artery (SIA), left- and right- sub-intestinal vein (SIV) located bilaterally atop the yolk and inter-connecting vessels (ICVs) which connect the SIA and SIV (Fig. 1A) and develops from angioblasts present within the ventral posterior cardinal vein, which give rise to both the SIA and the SIV (Goi and Childs, 2016; Hen et al., 2015; Koenig et al., 2016). The primitive SIVP expands bilaterally over the surface of the yolk and ECs from the primary SIV migrate dorsally throughout the plexus to form branches and the SIA (Goi and Childs, 2016; Hen et al., 2015; Koenig et al., 2016). Progressive refinement of a vascular network by vessel pruning or regression involves dynamic migration and rearrangement of ECs in mammals (Franco et al., 2015, 2016; Udan et al., 2013). ECs can migrate throughout patent blood vessels within a developing vascular network (Christ et al., 1990; Franco et al., 2015), and we therefore hypothesised that coordination of EC motility is critical during vascular remodelling of the SIVP and may be regulated by blood flow.

Vascular Endothelial Growth Factor (VEGF) signalling controls diverse aspects of EC biology, including co-ordination of migration and survival (Akeson et al., 2010; Ferrara et al., 2003). VEGF ligands signal via their cognate receptor tyrosine kinase receptors VEGFR1-3, with VEGFR2 being the main signalling VEGFR in mammalian blood endothelial cells (Simons et al., 2016). In zebrafish, Vegfr4/Kdrl and Vegfr2/Kdr are functionally conserved with mammalian VEGFR2 (Bussmann et al., 2008). ECs sense blood flow via junctional mechanosensory complexes, the best characterised being the VE-cadherin, PECAM-1, VEGFR2/3 mechanotransducer that functions independent of VEGF ligands and is required for arterial vascular remodelling (Coon et al., 2015; Tzima et al., 2005). Levels of endothelial VEGFR3/Flt4 establish a fluid shear stress set point and sustained deviations from this initiate vascular remodelling in arteries (Baeyens et al., 2015; Tzima et al., 2005). Zebrafish *vegfaa* mutants display profound disruption of SIVP formation (Habeck et al., 2002; Koenig et al., 2016). Combined loss-of-function of the VEGF receptors *kdrl* and *kdr* disrupt SIVP formation similar to that observed in *vegfaa* mutants (Habeck et al., 2002; Koenig et al., 2016) indicating Vegfaa signalling via Kdrl and Kdr promote SIVP development. By contrast, *vegfc* or *flt4* mutants display no apparent defects in SIVP formation (Hogan et al., 2009a, 2009b; Le Guen et al., 2014), although *vegfc* is sufficient to induce SIVP sprouting in a similar manner to *vegfaa* (Habeck et al., 2002; Koenig et al., 2016). Co-ordination of sprout pathfinding in the SIVP is dependent upon function of a guidance receptor, PlexinD1, and plexus growth is limited by inhibition of Bone Morphogenetic Protein (BMP) signalling (Goi and Childs, 2016). SIVP remodelling is known to occur via pruning of vessel branches and fusion of collateral vessels in a flow-dependent manner (Hen et al., 2015; Lenard et al., 2015). Interestingly, retraction of SIVP leading sprouts has been observed (Hen et al., 2015), leaving an unresolved question of whether this is dependent upon blood flow. In addition, a systematic characterisation of how EC migration is coordinated within the SIVP during plexus formation is lacking and how blood flow interacts with signalling pathways to co-ordinate plexus remodelling is yet to be discovered. Here we show the critical role of blood flow in coordinating EC migration during formation of a vascular plexus. Using time-lapse imaging and analysis of EC migration, we show that blood flow co-ordinates the collective migration of ECs throughout the developing vascular network of the SIVP, promotes regression of leading angiogenic sprouts to support plexus growth and limits the diameter of veins. Our data suggest that sprout regression occurs by coordinated rearrangement of ECs between non-perfused leading sprouts and the vessel lumen, mediated by directed EC polarisation and migration against blood flow. Using erythrocyte depletion to reduce blood flow throughout the plexus, we find that reduced circulation is compatible with normal sprout regression but insufficient to restrict vessel diameter. Notably, both remodelling processes depend on *flt4* function, indicating complex control of flow-responsive remodelling by this receptor. Collectively, these studies provide a clear view of the complex cellular behaviour underlying vessel remodelling during vascular plexus formation coordinated by the response of ECs to blood flow.

Methods

Zebrafish strains

Maintenance of zebrafish and experimental procedures involving zebrafish were carried out according to UK national guidelines and under UK Home Office licenses. The following zebrafish lines were employed in this study: *Tg(fli1a:*EGFP*)*^{y1} (Lawson and Weinstein, 2002)*, Tg(gata1a:*DsRed*)*^{sD2} (Traver et al., 2003), *Tg(fli1a:AC-TagRFP)*^{SH511}(Savage et al., 2019), *Tg(kdrl:EGFP)*^{s843} (Jin et al., 2005), *Tg(fli1a:nls*-mCherry*)*^{SH550} (this study), *Tg(fli1a:nls*-EGFP*)*^{SH549} (this study), *Tg(fli1a:golgi*-TagRFP*; cryaa:*CFP*)*^{SH529} (this study), *flt1*^{bns29} (Matsuoka et al., 2016).

Generation of Transgenic lines

Tg(fli1a:nls-EGFP*)*^{SH549} and *Tg(fli1a:nls-mCherry)*^{SH550} were generated using the Tol2 Kit (Kwan et al., 2007) via standard methods as previously described (Savage et al., 2019) using the following components: p5E-fli1aep (Villefranc et al., 2007), pME-mCherry or pME-EGFP, p3E-SV40pA, and pDestTol2-pA2. *Tg(fli1a:golgi-TagRFP, cryaa:cerulean)*^{SH529} was generated by fusing amino acids 1-60 of Human B4GALT1 to the N-terminus of TagRFP via *in silico* synthesis. attB1/attB2R sites were added to the fusion product by PCR (Supplementary Table 1) to generate pME-Golgi-TagRFP. The *fli1a:golgi*-TagRFP*; cryaa:*CFP construct was generated using the Tol2 Kit and the following components: p5E-fli1aep, pME-Golgi-TagRFP, p3E-SV40pA, and pDestTol2cryCFP. Embryos were injected at one-cell stage with 25 ng/µl *Tol2* mRNA and corresponding plasmid DNA.

Microinjection of morpholinos and mRNA

Microinjections were performed on single cell embryos with 1nl injection volume. Embryos were injected with 0.8ng morpholinos (Supplementary Table 1) including control, *tnnt2a* (Sehnert et al., 2002), *flt4* (Hogan et al., 2009), and *gata1a* (Galloway et al., 2005) or 200pg mRNA including *mTurquoise2* and *vegfaa*$_{165}$ (Lawson et al., 2002).

G0 *tnnt2a* CRISPR mutants

Target sequences were ordered as crRNAs (Merck) based on previously published sequences (Wu et al., 2018) (Supplementary Table 1) and co-injected alongside tracrRNA (Merck) in equimolar ratios and EnGen®Spy Cas9 NLS protein (NEB) into 1-cell zebrafish embryos.

RNA *in situ* hybridisation

Alkaline phosphatase wholemount *in situ* hybridisation experiments were performed using standard methods as described previously (Wilkinson et al., 2012) using probes against *mflt1* (Krueger et al., 2011), *sflt1* (Krueger et al., 2011), *flt4* (Thompson et al., 1998), *kdrl* (Fouquet et al., 1997). Detailed protocols are available upon request.

Live imaging of zebrafish embryos and larvae

Zebrafish were anaesthetised using Tricaine (MS-222, Sigma-Aldrich) and embedded in 1% low-melting point agarose which was held in place in a glass capillary and imaged using a light sheet Z.1 microscope (Zeiss). The chamber contained E3 and tricaine (164mg/L) to ensure embryos and larvae remained anaesthetised throughout imaging. Imaging was performed at 28.5°C. Images were acquired using ZEN software (Zeiss). Zebrafish were imaged at 5-minute intervals to detect blood flow, and 10-minute intervals to track EC nuclei. To image individual erythrocytes in *gata1a* morphants, time lapses were taken at 50 frames per second for 30 seconds with 1 µm z-stacks. The number of erythrocytes which passed a defined region of the SIV within a 30 second period were manually counted.

Quantification of SIVP morphology

Image quantification and analysis was performed using FIJI (Schindelin et al., 2012). Parameters employed to quantify SIVP morphology including area, length, vascular loops, sprout number and EC number, were recorded in a region of 5 somite widths. The length of the SIVP was measured as the vertical distance from the SIA to the most ventral part of the SIV. To ensure only endothelial nuclei within the SIVP were quantified, dual channel fluorescence was employed to highlight EC cytosol and nuclei. To quantify average SIV diameter, the SIV was measured at three equidistant points positioned anteroposteriorly and mean value was calculated.

EC rearrangement and cell trajectory analysis

Tg(fli1a:nls-mCherry*)*^{SH550} heterozygous embryos were used for cell tracking studies. Time-lapse images were pre-processed using Linear Stack Alignment with SIFT (Lowe, 2004) in FIJI and the movements of EC nuclei were tracked using TrackMate (Tinevez et al., 2017). Any misconnected tracks were manually corrected. Tracking data was exported and analysed using customised MATLAB scripts freely available at https://github.com/yanc0913/SIVP_cell_tracking. ECs were colour coded as tip cells (magenta), SIVP branches (orange), or SIV cells (blue) depending upon their initial position at the start of tracking (56 hpf). At the end of observation (72 hpf), cell positions were evaluated to determine whether ECs moved between EC subsets e.g., an EC initially located in the SIV which migrated to a branch by the end of tracking was recorded as a single rearrangement event. The number of ECs at initial and final position and the events of EC rearrangement were manually recorded from each time lapse. To analyse migration trajectory, a migration step was defined as one cell at position 1 (x_1 and y_1) migrating to its subsequent position 2 (x_2 and y_2) in a time range (from t_1 to t_2). The distance (or displacement) of the step (or the track) was calculated as $\sqrt{\Delta x^2 + \Delta y^2}$. Track distance was the sum of step displacements. Migration velocity was calculated as step displacement divided by time interval, and the mean velocity at a particular time range was the average of each velocity in that range. The

angle of each migration step was calculated using the four-quadrant inverse tangent (*atan2)* function in MATLAB, which computed the arctangent of Δy and Δx.

Quantification of EC Golgi polarity

In sprout cells, the position of the Golgi at either dorsal (45-135°) or ventral (225-315°) end of the elongated EC nucleus was considered polarised. In SIV cells, the position of the Golgi at either anterior (or downstream of blood flow, 135-180°) or posterior (or upstream of blood flow, 0-45°) end of the elongated EC nucleus was considered polarised.

Statistical analyses

Statistical analyses and graph plots were performed using GraphPad Prism 8. All statistical analysis is described in figure legends, including paired/unpaired *t*-test, ordinary one-way ANOVA, and two-way ANOVA. All error bars display the mean and standard deviation in the figures. *p*-values, unless exact value is listed, are as follows: *=<0.05, **=≤0.01, ***=≤0.001, ****=≤0.0001.

Results

Blood flow controls SIVP remodelling by influencing EC distribution and promoting leading sprout regression.

The SIVP develops from angiogenic sprouts which emerge from the posterior cardinal vein (PCV) by 30 hpf and migrate in a ventrolateral direction, bilaterally, over the surface of the yolk (Goi and Childs, 2016; Hen et al., 2015; Koenig et al., 2016). To determine the timing of SIVP development in relation to blood flow, we imaged the developing plexus in the presence of fluorescently labelled erythrocytes (Fig.1A). We find that blood flow entered the nascent SIV anteriorly from the supra-intestinal artery (SIA) between 53 hpf and 55 hpf (Fig. 1A-C"). The circulation perfused the developing SIVP from anterior to posterior and the plexus became fully perfused by 72 hpf (Fig. 1D-F", G supplementary movie 1). The SIVP undergoes extensive remodelling as the vascular network becomes perfused. Migrating angiogenic sprouts, hereafter referred to as leading sprouts, protrude from the ventral sub intestinal vein (SIV) and were observed to either undergo anastomosis with neighbouring sprouts or regress such that their constituent ECs became incorporated within the SIV by 70 hpf (Fig. 1H-J, arrows, supplementary movie 1 and 2, arrowheads).

Remodelling of leading sprouts was coincident with blood flow. In the SIVP, new sprouts are rarely produced after the onset of flow and most existing sprouts remodel via regression, therefore we considered the time after the onset of flow as the period of sprout regression. To determine whether this process was dependent upon blood flow, we inhibited cardiac contraction and circulation using a morpholino targeting cardiac troponin T type 2a (*tnnt2a*) (Sehnert et al., 2002) and examined SIVP

morphology (Fig. 2). The size of the SIVP was unchanged in *tnnt2a* morphants in comparison to controls, (Fig. 2A-B', C), however, SIVP morphology was altered in these larvae (Fig. 2A, B). Fewer vascular loops were present in *tnnt2a* morphants (Fig.2A', B' asterisks, D). In addition, *tnnt2a* morphants displayed reduced dorsoventral plexus length (Fig. 1A', B', E) but increased length (Fig. 2A', B', E) and number of leading sprouts (Fig. 2A", B", E, F). While the total EC number of the SIVP was not significantly different between *tnnt2a* morphants and controls (Fig. 2G), EC distribution was altered in *tnnt2a* morphants (Fig. 2A", B", H, I). Leading sprouts contained increased numbers of ECs in *tnnt2a* morphants (Fig. 2A", B", H, I), whereas SIVP branches contained significantly fewer ECs; however, EC frequency within the ventral region of the SIVP, the sub intestinal vein (SIV), was not significantly altered (Fig. 2A", B", I). To control for potential off target effects induced by morpholino injection, we created G0 *tnnt2a* CRISPR mutants (Wu et al., 2018) and assessed SIVP morphology. Plexus morphology in mosaic *tnnt2a* CRISPR mutants was abnormal (Fig. S1A, B arrows, C-I) and phenocopied that of *tnnt2a* morphants (Fig. 2), indicating these defects were specific to inhibition of *tnnt2a* function. Collectively, this suggests that blood flow influences EC distribution throughout the developing venous plexus without altering the total number of ECs within the plexus. Moreover, the increased size and frequency of leading sprouts in *tnnt2a* morphants suggests blood flow may promote regression of these vessels. Consistent with this, leading sprouts underwent regression in the presence of blood flow and their ECs became incorporated into the SIV (Fig. 3A-C, arrows, Supplementary Movie 3). By contrast, the number of regressing sprouts was significantly reduced in *tnnt2a* morphants and larvae possessed more leading sprouts than controls by 72 hpf. Anastomosis of leading sprouts was rare and occurred independently of blood flow (Fig. 3A, asterisk, G, H, Supplementary movie 3). Taken together, these data indicate that blood flow influences SIVP remodelling in part by promoting regression of leading sprouts.

Blood flow controls EC migration but not proliferation within the developing SIVP

The distribution of ECs within a developing plexus could be influenced by a variety of mechanisms, including differential EC proliferation, apoptosis, or migration. While the total number of ECs within the SIVP did not alter in the absence of flow (Fig. 2G), it remained possible that the altered distribution of ECs observed could result from differential rates of proliferation/apoptosis throughout the plexus and that this may be influenced by flow. To examine whether differential EC proliferation, apoptosis, or migration contributed to the altered EC distribution of plexuses which developed in the absence of blood flow (Fig. 2I), we tracked ECs within the developing SIVP in control and *tnnt2a* morphants from 56-70 hpf (Fig. 4, Supplementary Movie 4, 5). Similar numbers of ECs were tracked at the beginning of each time-lapse and ECs were grouped according to their location at 56hpf, either within SIVP branches, SIV, or tip cells within leading sprouts (Fig. 4A-B).

Endothelial proliferation was unaffected by the flow status of the developing plexus (Fig. 4C) and no apoptotic events were observed during SIVP development in either the presence or absence of blood flow. Thus, differential proliferation or apoptosis were unlikely to account for altered EC distribution observed in *tnnt2a* morphants (Fig. 2I). However, the frequency with which ECs differentially contributed to neighbouring EC subsets was altered in the absence of blood flow (Fig. 4D). In the presence of blood flow, 73% of leading sprouts consisted of a pair of endothelial tip cells positioned in parallel to each other, which is consistent with previous reports (Hen et al., 2015). When tip cells divided in the presence of blood flow (Fig. 4B), in most cases (77%), the dorsal daughter cell underwent rapid dorsal migration to contribute to the SIV (Supplementary Movie 6, arrows), leaving only the paired tip cells within the sprout and suggesting these daughter cells adopted a stalk identity (Supplementary Table 2). In rare cases in the presence of blood flow (<2%), daughter cells within sprouts which underwent dorsal migration to the SIV subsequently contributed to SIVP branches by 72 hpf (Fig. 4D). ECs were not observed to migrate into leading sprouts in the presence of blood flow, however, occasionally the nucleus of ECs at the boundary between the SIV and leading sprouts were observed to bend and transiently shuffle their position between the SIV and sprout. By contrast, only 25% of tip cells migrated dorsally to contribute to the SIV in the absence of blood flow and most tip cells remained within the leading sprout by 72 hpf. This is consistent with the observation that *tnnt2a* morphants displayed increased numbers of ECs within leading sprouts (Fig. 2B”, I, S1I). However, SIV ECs were observed to migrate ventrally to contribute to leading sprouts in *tnnt2a* morphants (Fig. 4D). Interestingly, SIV cells which underwent ventral migration into sprouts in *tnnt2a* morphants were not observed to compete with the tip cells at the migration front of the sprout, suggesting these ECs did not acquire tip cell characteristics within the sprouts.

ECs within SIVP branches comprise half of the total cell population of the SIVP but displayed only rare positional changes towards other EC subsets in the presence of blood flow, such that fewer than 1% of ECs within SIVP branches contributed to cellular rearrangement of the SIVP (Supplementary Table 2, Fig. 4D). By contrast, EC contribution to the SIV from branches was significantly increased in *tnnt2a* morphants (Fig. 4D). The total number of EC positional change events between control and *tnnt2a* morphants was not significantly different (Figure 4D), however, ECs tended to migrate more dorsally throughout the plexus in the presence of flow, whereas ventral migration of ECs was increased in those plexuses which developed without blood flow (Fig. 4D). Collectively, these data indicate that blood flow is required for directed rearrangement of ECs during SIVP development. In the presence of blood flow, ECs in the SIVP displayed distinct migratory behaviours depending upon their position. While the SIVP expanded and ECs migrated ventrally, blood flow promoted dorsal migration of ECs, presumably to support the expansion of the plexus (Fig. 4E). In contrast, in the absence of blood flow, SIVP ECs displayed persistent ventral cell movement, resulting in distended SIVP branches which contained fewer cells (Fig. 3C, F) and elongated leading sprouts with an accumulation of ECs (Fig. 4E).

Blood flow co-ordinates direction of EC migration during SIVP development

During cellular rearrangement within the SIVP, ECs displayed distinct migration behaviours depending upon the flow status of the plexus and their position within it (Fig. 4D). Thus, we sought to establish whether blood flow can influence the ability of ECs to migrate within the SIVP. Considering the SIVP displays a curvature approximating a semi-circle, ECs in the anterior and posterior of the SIVP migrate shorter distances than the most ventral cells in the centre of the plexus. Therefore, we tracked the most ventral ECs in each SIVP and focused on ECs within the SIV and sprouts (Fig. 5A). We examined the trajectories and migration paths of ECs within the SIV and leading sprouts (Fig. 5A) by analysing EC movement between consecutive timepoints (Fig. 5B, black arrows), hereafter referred to as migration steps. ECs close to the most ventral sprout of each SIVP were grouped into SIV ECs (blue) or tip cells (magenta) according to their initial position at 56 hpf (Fig. 5A, B) and each migration step was recorded at 30 min intervals. The total distance each cell migrated in control or *tnnt2a* morphants was not significantly different (Fig. 5C), however, the net distance travelled during each time-lapse, hereafter referred to as meandering index (distance/displacement ratio), was significantly reduced in tip cells in *tnnt2a* morphants (Fig. 5D). The closer the meandering index is to 1, the straighter the migration path of the cells and values >1 indicate increased tortuosity of migration. Thus, in *tnnt2a* morphants, tip cells showed a more directed migration path ventrally in the absence of blood flow (Fig. 5D) indicating less dorsal rearrangement towards the SIV. By contrast, the meandering index of ECs within the SIV was not significantly affected by the flow status of the plexus (Fig. 5E). Migration velocity of Tip and SIV ECs gradually reduced in the presence of blood flow, whereas in *tnnt2a* morphants, there was no significant reduction in migration velocity (Fig. 5F), indicating blood flow may act to progressively slow the migration of ECs and promote vessel stability. Spacing of EC nuclei was reduced in *tnnt2a* morphants (Fig. 5G) consistent with increased EC density in the absence of blood flow (Fig. 2B”).

The co-ordinates of tip EC migration steps fell within a 5µm radius in both control and *tnnt2a* morphants (Fig. 5H, I, magenta circle). Migration step co-ordinates in *tnnt2a* morphant tip ECs, were more confined along the y-axis compared to controls (Fig 5H, I magenta circle), reflecting increased crowding of ECs within sprouts (Fig. 5G) and significantly reduced dorsal but increased ventral migration (Fig. 5J). The co-ordinates of SIV EC migration steps (Fig. 5K) were similar to tip cells in the presence of flow (Fig. 5H), reflecting that tip and SIV cells were in close contact and migrated collectively during SIV development. However, SIV ECs in *tnnt2a* morphants displayed a significant anterior migration bias (Fig. 5K, L, M). Taken together, these data suggest blood flow biases direction of EC migration. During SIVP development, while all ECs migrate collectively towards a ventral-anterior direction as the plexus expands, the onset of flow provides a directionality cue, biasing migration towards the posterior in SIV cells against the direction of blood flow and promoting dorsal migration of tip ECs, resulting in regression of leading sprouts and incorporation of tip ECs within the SIV (Fig. 5K). Thus, in the presence of blood

flow, SIV cells migrate laterally to accommodate dorsally migrating tip cells within the SIV as leading sprouts regress. By contrast, in the absence of flow, SIV ECs migrate more anteriorly, and tip cells migrate ventrally leading to elongated sprouts and failure of regression. Considering blood flows along the SIV from posterior to anterior (Fig. 1), this suggests that blood flow likely provides a horizontal force against which SIVP ECs migrate.

Blood flow polarises ECs to initiate reverse migration during sprout regression

During vascular development, ECs polarise during migration and in response to blood flow (Franco et al., 2015; Kwon et al., 2016). Venous ECs are often less polarised than arterial ECs (Kwon et al., 2016). Therefore, to determine whether SIVP ECs become polarised in response to flow during sprout regression, we employed transgenic lines *Tg(fli1a:nls-EGFP)*^{SH549} and *Tg(fli1a:golgi-tagRFP, cryaa:CFP)*^{SH529} to label endothelial nuclei and Golgi respectively within the SIVP (Fig. S2A-B). We imaged the SIVP in control and *tnnt2a* morphants at the onset of flow (56hpf) and during sprout regression (64 hpf) and quantified the relative position of the nuclei and Golgi located within ECs of leading sprouts and SIV.

Before the onset of blood flow, most tip cells displayed ventral Golgi positioning at the migration front with a minority polarised dorsally (Fig. S2B). The frequency of dorsal polarisation did not significantly alter in *tnnt2a* morphants (Fig. S2B). Similarly, most SIV cells were non-polarised before the onset of flow in controls and there was no significant difference in EC polarity observed in *tnnt2a* morphants (Fig. S2C). By 64 hpf, once the SIVP was perfused, the proportion of tip cells with dorsally positioned Golgi was significantly reduced in *tnnt2a* morphants. This is consistent with observations that tip cells underwent persistent ventral migration in the absence of flow, but in the presence of flow, these tended to migrate dorsally throughout the SIVP (Fig. 5J). By 64 hpf, the proportion of SIV ECs polarised upstream of flow was significantly increased in controls in comparison to *tnnt2a* morphants (Fig. S2C). These data are consistent with our cell tracking (Fig. 5) and suggest blood flow provides a directionality cue to co-ordinate EC migration within the SIVP and initiate sprout regression.

To investigate how EC rearrangement occurred during sprout regression, we labelled the endothelial actin cytoskeleton and imaged ECs in regressing sprouts using an EC-specific actin nanobody line, *Tg(fli1a:AC-TagRFP)* (Savage et al., 2019) (Fig. S3 & Supplementary Movie 7). Leading sprouts consisted of a pair of tip cells with their dorsal membranes connected with the SIV lumen (Fig. S3A-D). As sprouts regressed, both tip cells crawled over each other toward the SIV. The tip cell at the front of the sprout (Fig. S3E-H, green) reoriented its nucleus from dorsoventral to lateral orientation with most of its membrane incorporated into the perfused SIV. The neighbouring tip cell (Fig. S3I-L, pink) followed the adjacent tip cell (Fig. S3I-L, green), retracting its membrane and re-orienting its nucleus horizontally

once it had reached the SIV. Meanwhile the adjacent tip cell (green) held its position, possibly to maintain SIV integrity. During sprout regression, an F-actin positive focus was observed to form at the ventral membrane of the trailing tip cell (Fig. S3H). This actin focus progressed to a ring structure which increased in size and eventually closed as the tip cell membrane converged into the main vessel (Fig. S3M-P, pink), suggesting involvement of dynamic actin reorganisation during regression. Collectively, these observations indicate the dorsal membrane of sprout ECs are in contact with blood flow within the SIV lumen during regression, consistent with a role for blood flow in induction of sprout regression. Furthermore, these observations suggest delicate collaboration between neighbouring tip cells ensures sprout regression without compromising vessel integrity.

Leading sprout regression occurs under conditions of reduced blood flow

EC rearrangement from regions of low to high shear stress has been implicated in vessel pruning within developing blood vessels (Franco et al., 2015). Shear stress experienced by ECs relates directly to haemodynamic flow and blood viscosity and inversely to the third power of arterial radius (Heil and Schaper, 2004). Since leading sprouts within the SIVP were not perfused and because tip cells within sprouts normally migrated towards the SIV, which was perfused (Fig. 1H-J), we next investigated whether reduced blood viscosity would be compatible with normal sprout regression. Reduction of blood viscosity was achieved by titration of *gata1a* morpholino to a level which substantially reduced circulating erythrocytes by 87% on average (Fig. 6A-C, arrowheads). Unlike *tnnt2a* loss-of-function (Fig. 2, S1), SIVP morphology in *gata1a* morphants was not substantially altered (Fig. 6A, B) such that ICVs remained connected with the SIA and the number of vascular loops remained unchanged (Fig. 6D). Many ICVs were not patent in *gata1a* morphants (Fig. 6B), likely due to fewer erythrocytes circulating through these vessels and this may have contributed to the reduced size of the plexus in these larvae (Fig. 6E, F). Surprisingly, there were no significant differences in the number of leading sprouts between control and *gata1a* morphants (Fig. 6G), which indicates that conditions of very low blood flow are compatible with normal sprout regression in the SIVP. In arteries, low shear stress generally induces inward remodelling as a mechanism to increase flow by constricting vessels (Silver and Vita, 2006). Surprisingly, SIV diameter was increased in *gata1a* morphants (Fig. 6F), indicating the SIV underwent expansive remodelling under conditions of reduced blood viscosity. Taken together, this suggests sprout regression can occur under conditions of reduced blood viscosity and is consistent with models which propose that the endothelial shear stress set point is low (Baeyens et al., 2015). Since SIV diameter increased in *gata1a* morphants, flow might act differently during venous remodelling than it does in arteries. We next sought to investigate whether mechanisms to sense changes in blood flow may be shared between arteries and veins.

Leading sprout regression and expansive venous remodelling is dependent on *flt4* under low blood flow conditions

Zebrafish *vegfr4*/*kdrl* and *vegfr2*/*kdr* are required individually and co-operatively for normal SIV formation (Habeck et al., 2002; Koenig et al., 2016). Sustained deviations in shear stress from the set-point induce vascular remodelling in zebrafish arteries via *flt4* (Baeyens et al., 2015). In addition, VEGFR1, also known as Flt1, inhibits venous hypersprouting within the CNS (Krueger et al., 2011; Matsuoka et al., 2016; Wild et al., 2017) and may function as a VEGF decoy receptor to limit angiogenesis (Hiratsuka et al., 1998; Park et al., 1994; Zygmunt et al., 2011). Increased SIVP sprouts have been described previously in *flt1* morphants (Hen et al., 2015) and while the flow status of the SIVP was not investigated in these studies, we reasoned that flow may promote *flt1* expression in the SIVP to facilitate regression. We first examined VEGF receptor expression in the SIVP in the presence and absence of blood flow. Expression of membrane-bound *flt1* (*mflt1*) was not detectable in the SIVP in the presence or absence of flow at 56 hpf when sprouts normally begin to regress (Fig. S4A, B), or by 72 hpf as regression completes (Fig S4C, D). Similarly, soluble *flt1* (*sflt1*) was not detectable in the SIVP at 56 hpf at the onset of regression in either the presence or absence of flow (Fig. S4E, F). However, while *sflt1* was not detected in the SIVP at 72 hpf in the presence of flow, it was present in the SIVP in 40% of *tnnt2a* morphants at this stage (Fig. S4G, H, arrow), suggesting flow may negatively regulate *flt1* expression within the SIVP. Consistent with this, while expression of *sflt1* was present and unaltered in the cerebral vasculature at 56 hpf in the presence or absence of flow (Fig. S4I, J, arrows), by 72 hpf *sflt1* expression was downregulated throughout the cerebral vasculature but *sflt1* expression persisted in the cerebral vasculature of *tnnt2a* morphants (Fig. S4K, L, arrows). Since *flt1* was not expressed within the developing SIVP in the presence of blood flow this would exclude a requirement for *flt1* during leading sprout regression. Consistent with this, sprout regression was normal in *flt1* mutants (Fig. S5A-F). Collectively, this suggests *flt1* is dispensable for sprout regression.

Kdrl is essential for normal SIVP formation and perfusion (Habeck et al., 2002) and Vegfr3/Flt4 has been proposed to function as a mechanosensor which regulates the endothelial shear stress set point (Baeyens et al., 2015). Expression of both *kdrl* and *flt4* was widespread throughout the developing SIVP (Fig. S6A-L, arrows) and their expression was retained in leading sprouts which failed to regress in *tnnt2a* morphants (Fig. S6I-L, arrows). Expression of *kdrl* was unaffected by the flow status of the plexus at all stages examined (Fig. S6A, B, E, F, I, J, arrows), whereas *flt4* expression was elevated throughout the ventral SIVP at 72 hpf in *tnnt2a* morphants in comparison to controls (Fig. S6K, L, green arrows). *flt4* expression was reduced in controls which underwent normal sprout regression and was also retained in leading sprouts which failed to regress in the absence of blood flow (Fig. S6K, L arrows). Since loss of *kdrl* function precludes formation of an intact perfused SIVP (Habeck et al., 2002; Koenig et al., 2016) we instead focused on *flt4 since flt4* loss-of-function has been shown to reduce arterial

caliber in zebrafish (Baeyens et al., 2015). Knockdown of *flt4* was compatible with leading sprout regression in a similar manner to *gata1a* morphants (Fig. 7A-E, arrows), however, knockdown of both *flt4* and *gata1a* induced incomplete sprout regression by 72 hpf in comparison to controls (Fig. 7D, arrows, E). Collectively, this indicates that while *flt4* is dispensable for sprout regression in the SIVP under physiological blood flow (Fig. 7C, E), its function is essential for regression of leading sprouts under low blood flow conditions (Fig. 7D, E).

Discussion

Developmental remodelling of vascular networks has been described in different models and has mainly focused on pruning of vascular cross branches (Chen et al., 2012; Franco et al., 2015; Kochhan et al., 2013; Lobov et al., 2011; Phng et al., 2009). In this context, pruning occurs in loop forming or cross branch vessel segments, which ultimately leads to regression of the cross branch, leaving behind the two parallel vessels via a process involving EC migration and apoptosis (Chen et al., 2012; Zhang et al., 2018). Dynamic EC migration and rearrangement have also been described in sprouts, however studies have mostly focused on angiogenic sprouting and anastomosis (Arima et al., 2011; Bentley et al., 2014; Jakobsson et al., 2010). Whether sprouts ultimately anastomose with each other, or not, and how these sprouts are remodelled, remained unknown. Here using the zebrafish SIVP we find most leading sprouts within the developing plexus are remodelled via EC migration-driven regression rather than anastomosis. Apoptosis during pruning has been described in murine retinal vessels when circulation is compromised (Franco et al., 2015, 2016; Hughes and Chan-Ling, 2000) and also in zebrafish cranial arteries (Kochhan et al., 2013; Zhang et al., 2018) but this has not been implicated during branch pruning within the SIVP (Lenard et al., 2015). Consistent with this, we tracked approximately 70% of SIVP ECs per plexus and while we cannot exclude the possibility that EC apoptosis occurs in the most anterior or posterior SIVP, or in the SIA, we observed no apoptotic events following live imaging of over 100 leading sprouts. Therefore, our data suggest that EC migration represents the primary mechanism of sprout regression within the SIVP. Indeed, angiogenic regression is an efficient system because cells are recycled via migration from sprouts, which are temporary structures, to other more permanent structures within developing vessels. Thus, co-ordination of EC migration represents a more efficient use of resources than sculpting vascular networks by proliferation or apoptosis.

Haemodynamic force exerted by blood flow has been proposed to be crucial in selecting and triggering pruning and regression of particular vessels (Chen et al., 2012; Franco et al., 2015; Kochhan et al., 2013; Lenard et al., 2015; Lucitti et al., 2007). Pruning mostly occurs in small and bifurcated branches with relatively unstable, or low, blood flow in comparison to adjacent large vessels (Chen et al., 2012; Lenard et al., 2015). This observation suggests that pruning is triggered by local differences in flow patterns between branches, which in turn induce EC polarisation and direct EC migration against flow,

from low-flow to high flow vessels (Franco et al., 2015). Our data are consistent with this and upon initiation of sprout regression within the SIVP, ECs within the non-perfused leading sprouts are likely 'attracted' by the relatively high flow in the SIV, these polarise and migrate out of the regressing sprouts and subsequently contribute to the SIV. In line with this, dorsal-lateral polarisation and migration-induced EC rearrangement are highly dynamic processes during sprout regression and are dependent on blood flow. Interestingly, ventral EC migration persisted throughout the SIVP in *tnnt2a* morphants which indicates a flow-independent mechanism controls this aspect of EC migration. While blood flow co-ordinates remodelling of the SIVP during development, the plexus forms a stereotypical basket-like structure consisting of well-defined branches, SIV and leading sprouts even in the absence of flow. This suggests SIVP formation is regulated by well-orchestrated molecular patterning cues which may interact with physical forces such as blood flow to refine plexus development. Indeed, loss of guidance molecules such as PlexinD1 disrupt SIVP patterning (Goi and Childs, 2016) and PlexinD1 has recently been identified as a shear stress mechanosensor in ECs (Mehta et al., 2020), however, it is unclear whether plexinD1 modulates EC response to flow during SIVP remodelling.

Remodelling of blood vessels from a primitive structure into a more mature network at onset of flow allows temporal separation of sprouting at the migration front from pruning of branches during angiogenesis (Lenard et al., 2015). In the SIVP, new sprouts are rarely produced after the onset of flow and most existing sprouts remodel via regression. While the entire plexus expands ventrally during this period, the tip cells within leading sprouts do not simply undergo initial ventral migration followed by dorsal migration during regression, rather these ECs display transient and stochastic dorsal migration steps while undergoing collective, flow-independent, ventral migration. This suggests that sprouting and regression are interlinked. An intriguing question is at which point such steps lead to irreversible sprout regression? One possibility is when the tip cells in the sprout come into direct contact with blood flow. At the onset of flow, the posterior membrane of the tip cells are connected with adjacent SIV ECs and have limited exposure to blood flow within the SIV. It is possible that when blood flow creates sufficiently high shear forces on the SIV cells, it drives their migration against flow, and this may exert a pulling force on the tip cells which could promote their dorsal-lateral migration and induce sprout regression. The SIV cells and the tip cells in contact with flow could act as the bridging ECs to sense differences in the local flow environment, as occurs during branch pruning (Franco et al., 2015). That the combined plexus and sprout length in *tnnt2a* morphants was not significantly different to controls indicates that in the absence of blood flow, ECs within sprouts can migrate the same distance as in controls. Reduced plexus length in the absence of blood flow is therefore a consequence of increased contribution of ECs from the branches and SIV to leading sprouts. In the presence of blood flow, ECs within sprouts migrate against flow and contribute to the SIV and branches, thereby supporting their expansion or growth. This is consistent with reports that ECs incorporate in developing arterial networks in the retina and coronary vasculature via coordinated EC migration (Chang et al., 2017; Pitulescu et al., 2017). Our data therefore

suggest blood flow promotes regression of leading sprouts within the SIVP as a mechanism to support expansion of the developing plexus. Moreover, sprouting and regression share similar cellular behaviours but in a 'reverse mode'.

Yolk sac vascular remodelling is dependent upon erythroblast circulation (Lucitti et al., 2007) and uneven erythrocyte distribution in bifurcations has been posited to enhance local shear stress differences between vessels undergoing pruning and their neighbouring vessels (Zhou et al., 2020). Thus, blood viscosity is strongly associated with vessel regression. How ECs sense low levels of flow remains unclear, but several possible molecular mechanisms have been proposed. The level of VEGFR3 has been suggested to maintain a threshold of shear stress sensed by ECs (Baeyens et al., 2015). Interaction of the transforming growth factor β (TGFβ) receptor, activin receptor like kinase ACVRL1/ALK1 with a component of the TGFβ receptor complex, Endoglin, has been reported to enhance EC sensitivity of flow sensing (Baeyens et al., 2016). In addition, non-canonical Wnt signalling may control vessel regression by modulating the threshold for flow-induced EC polarisation (Franco et al., 2016). We find that while plexus length was reduced in erythrocyte depleted embryos, even substantial reductions in blood viscosity were compatible with sprout regression. We find that sprout regression in the SIVP is dependent upon *flt4* under these reduced flow conditions, but *flt4* function is dispensable for sprout regression under normal blood flow. This indicates additional mechanisms could be involved to regulate sprout regression under normal flow conditions. Consistent with this, *flt4* mutants display normal SIVP formation (Hogan et al., 2009a, 2009b), suggesting different function of Flt4 under different flow conditions in zebrafish. The established role of VEGFR2 during EC mechanosensation (Coon et al., 2015; Tzima et al., 2005) suggests Kdr and Kdrl are promising candidates to mediate sprout regression under normal flow, however, their requirement during SIVP formation precluded their assessment in this study. The redundant function of Flt4 during sprout regression imparts robustness on the system and facilitates proper vessel remodelling under dysregulated flow conditions. It is important to note that while SIVP leading sprouts are not perfused before or during their regression, a low level of shear provided by skimmed plasma could promote dorsal migration of tip cells to elicit regression (Zhou et al., 2020).

Conditional deletion of *Vegfr3* in mice and knockdown of *flt4* in zebrafish embryos reduced arterial lumen diameter, suggesting *flt4* promotes expansive outward remodelling of arteries in response to flow (Baeyens et al., 2015). We find that in addition to promoting sprout regression under conditions of reduced blood flow, *flt4* also promotes outward remodelling of the SIV. These results indicate that arteries and veins share common molecular mechanisms which mediate vascular remodelling in response to flow. This study raises important questions of how the mechanosensory input from altered blood flow is transduced by Flt4 to elicit the cytoskeletal changes necessary to rapidly adjust EC

544 migration. Moreover, how these mechanisms enable Flt4 to co-ordinate distinct aspects of remodelling
545 such as promoting expansive venous remodelling while co-ordinating migration during regression
546 require further investigation.
547

548 **Acknowledgements**

549 We would like to thank the aquarium staff at the University of Sheffield and University of Nottingham
550 for excellent zebrafish husbandry. We thank Freek van Eeden for helpful discussions, Didier Stainier
551 for providing the *flt1* mutant and Tim Chico for *tnnt2a* morpholino. This work was supported by a
552 China Scholarship Council and University of Sheffield joint studentship to YC, JG Graves Medical
553 Research Fellowship and Nottingham Research Fellowship to RNW, Diabetes UK (17/0005678 to
554 RNW), BBSRC (BB/R015457/1 to RNW) and British Heart Foundation (RG/19/10/34506 to PCE).
555

556 **Author Contribution**

557 RNW and PCE conceived the project. YC, ZJ, KHF, HRK, PCE, RNW designed experiments; YC, ZJ,
558 HRK performed experiments, YC, ZJ, RNW analysed data, RNW wrote the manuscript and all authors
559 reviewed the final manuscript.
560

561 **Conflicts of Interest**

562 The authors declare no conflicts of interest
563

564 **References**

565 Akeson, A., Herman, A., Wiginton, D., and Greenberg, J. (2010). Endothelial cell activation in a
566 VEGF-A gradient: relevance to cell fate decisions. Microvasc. Res. *80*, 65–74.

567 Arima, S., Nishiyama, K., Ko, T., Arima, Y., Hakozaki, Y., Sugihara, K., Koseki, H., Uchijima, Y.,
568 Kurihara, Y., and Kurihara, H. (2011). Angiogenic morphogenesis driven by dynamic and
569 heterogeneous collective endothelial cell movement. Development *138*, 4763–4776.

570 Baeyens, N., Nicoli, S., Coon, B.G., Ross, T.D., van den Dries, K., Han, J., Lauridsen, H.M., Mejean,
571 C.O., Eichmann, A., Thomas, J.-L., et al. (2015). Vascular remodeling is governed by a VEGFR3-
572 dependent fluid shear stress set point. Elife *4*.

573 Baeyens, N., Larrivée, B., Ola, R., Hayward-Piatkowskyi, B., Dubrac, A., Huang, B., Ross, T.D.,
574 Coon, B.G., Min, E., Tsarfati, M., et al. (2016). Defective fluid shear stress mechanotransduction
575 mediates hereditary hemorrhagic telangiectasia. J. Cell Biol. *214*, 807–816.

576 Bentley, K., Franco, C.A., Philippides, A., Blanco, R., Dierkes, M., Gebala, V., Stanchi, F., Jones, M.,
577 Aspalter, I.M., Cagna, G., et al. (2014). The role of differential VE-cadherin dynamics in cell
578 rearrangement during angiogenesis. Nat. Cell Biol. 1–15.

579 Bussmann, J., Lawson, N., Zon, L., Schulte-Merker, S., and Committee, Z. N. (2008). Zebrafish VEGF
580 receptors: a guideline to nomenclature. PLoS Genet. *4*, e1000064.

581 Campinho, P., Vilfan, A., and Vermot, J. (2020). Blood Flow Forces in Shaping the Vascular System:
582 A Focus on Endothelial Cell Behavior. Front. Physiol. *11*, 552.

583 Chang, A.H., Raftrey, B.C., D'Amato, G., Surya, V.N., Poduri, A., Chen, H.I., Goldstone, A.B., Woo,
584 J., Fuller, G.G., Dunn, A.R., et al. (2017). DACH1 stimulates shear stress-guided endothelial cell
585 migration and coronary artery growth through the CXCL12-CXCR4 signaling axis. Genes Dev. *31*,
586 1308–1324.

587 Chen, Q., Jiang, L., Li, C., Hu, D., Bu, J., Cai, D., and Jiu-lin (2012). Haemodynamics-driven
588 developmental pruning of brain vasculature in zebrafish. PLoS Biol. *10*, e1001374.

589 Christ, B., Poelmann, R.E., Mentink, M.M., and Gittenberger-de Groot, A.C. (1990). Vascular
590 endothelial cells migrate centripetally within embryonic arteries. Anat. Embryol. *181*, 333–339.

591 Coon, B.G., Baeyens, N., Han, J., Budatha, M., Ross, T.D., Fang, J.S., Yun, S., Thomas, J.-L., and
592 Schwartz, M.A. (2015). Intramembrane binding of VE-cadherin to VEGFR2 and VEGFR3 assembles
593 the endothelial mechanosensory complex. J. Cell Biol. *208*, 975–986.

594 Ferrara, N., Gerber, H., and LeCouter, J. (2003). The biology of VEGF and its receptors. Nat. Med. *9*,
595 669–676.

596 Fouquet, B., Weinstein, B.M., Serluca, F.C., and Fishman, M.C. (1997). Vessel patterning in the
597 embryo of the zebrafish: guidance by notochord. Dev. Biol. *183*, 37–48.

598 Franco, C.A., Jones, M.L., Bernabeu, M.O., Geudens, I., Mathivet, T., Rosa, A., Lopes, F.M., Lima,
599 A.P., Ragab, A., Collins, R., et al. (2015). Dynamic endothelial cell rearrangements drive
600 developmental vessel regression. PLoS Biol. *13*, e1002125.

601 Franco, C.A., Jones, M.L., Bernabeu, M.O., Vion, A.-C., Barbacena, P., Fan, J., Mathivet, T.,
602 Fonseca, C.G., Ragab, A., Yamaguchi, T.P., et al. (2016). Non-canonical Wnt signalling modulates
603 the endothelial shear stress flow sensor in vascular remodelling. Elife *5*.

604 Galloway, J.L., Wingert, R.A., Thisse, C., Thisse, B., and Zon, L.I. (2005). Loss of gata1 but not gata2
605 converts erythropoiesis to myelopoiesis in zebrafish embryos. Dev. Cell *8*, 109–116.

606 Goi, M., and Childs, S. (2016). Patterning Mechanisms of the Sub-Intestinal Venous Plexus in
607 Zebrafish. Dev. Biol. 409, 114-128.

608 Habeck, H., Odenthal, J., Walderich, B., Maischein, H.-M., and Schulte-Merker, S. (2002). Analysis of
609 a Zebrafish VEGF Receptor Mutant Reveals Specific Disruption of Angiogenesis. Curr. Biol. *12*, 1405-
610 1412.

611 Heil, M., and Schaper, W. (2004). Influence of mechanical, cellular, and molecular factors on
612 collateral artery growth (arteriogenesis). Circ. Res. *95*, 449–458.

613 Hen, G., Nicenboim, J., Mayseless, O., Asaf, L., Shin, M., Busolin, G., Hofi, R., Almog, G., Tiso, N.,
614 Lawson, N.D., et al. (2015). Venous-derived angioblasts generate organ-specific vessels during
615 zebrafish embryonic development. Development *142*, 4266–4278.

616 Hiratsuka, S., Minowa, O., Kuno, J., Noda, T., and Shibuya, M. (1998). Flt-1 lacking the tyrosine
617 kinase domain is sufficient for normal development and angiogenesis in mice. Proc. Natl. Acad. Sci.
618 U. S. A. *95*, 9349–9354.

619 Hogan, B.M., Bos, F.L., Bussmann, J., Witte, M., Chi, N.C., Duckers, H.J., and Schulte-Merker, S.
620 (2009a). Ccbe1 is required for embryonic lymphangiogenesis and venous sprouting. Nat. Genet. *41*,
621 396–398.

622 Hogan, B.M., Herpers, R., Witte, M., Heloterä, H., Alitalo, K., Duckers, H., and Schulte-Merker, S.
623 (2009b). Vegfc/Flt4 signalling is suppressed by Dll4 in developing zebrafish intersegmental arteries.
624 Development *136*, 4001–4009.

Hughes, S., and Chan-Ling, T. (2000). Roles of endothelial cell migration and apoptosis in vascular remodeling during development of the central nervous system. Microcirculation *7*, 317–333.

Isogai, S., Horiguchi, M., and Weinstein, B.M. (2001). The vascular anatomy of the developing zebrafish: an atlas of embryonic and early larval development. Dev. Biol. *230*, 278–301.

Jakobsson, L., Franco, C.A., Bentley, K., Collins, R., Ponsioen, B., Aspalter, I.M., Rosewell, I., Busse, M., Thurston, G., Alex, et al. (2010). Endothelial cells dynamically compete for the tip cell position during angiogenic sprouting. Nat. Cell Biol. *12*, 943–953.Kochhan, E., Lenard, A., Ellertsdottir, E., Herwig, L., Affolter, M., Belting, H.-G., and Siekmann, A.F. (2013). Blood Flow Changes Coincide with Cellular Rearrangements during Blood Vessel Pruning in Zebrafish Embryos. PLoS One *8*, e75060.

Koenig, A.L., Baltrunaite, K., Bower, N.I., Rossi, A., Stainier, D., Hogan, B.M., and Sumanas, S. (2016). Vegfa signaling promotes zebrafish intestinal vasculature development through endothelial cell migration from the posterior cardinal vein. Dev. Biol.

Korn, C., and Augustin, H.G. (2015). Mechanisms of Vessel Pruning and Regression. Dev. Cell *34*, 5–17.

Krueger, J., Liu, D., Scholz, K., Zimmer, A., Shi, Y., Klein, C., Siekmann, A., Schulte-Merker, S., Cudmore, M., Ahmed, A., et al. (2011). Flt1 acts as a negative regulator of tip cell formation and branching morphogenesis in the zebrafish embryo. Development *138*, 2111–2120.

Kwan, K.M., Fujimoto, E., Grabher, C., Mangum, B.D., Hardy, M.E., Campbell, D.S., Parant, J.M., Yost, H.J., Kanki, J.P., and Chien, C. (2007). The Tol2kit: a multisite gateway-based construction kit for Tol2 transposon transgenesis constructs. Dev. Dyn. *236*, 3088–3099.

Kwon, H.-B., Wang, S., Helker, C., Rasouli, S.J., Maischein, H.-M., Offermanns, S., Herzog, W., and Stainier, D. (2016). In vivo modulation of endothelial polarization by Apelin receptor signalling. Nat. Commun. *7*, 11805.

Jin, S.-W., Beis, D., Mitchell, T., Chen, J.-N., and Stainier, D. (2005). Cellular and molecular analyses of vascular tube and lumen formation in zebrafish. Development *132*, 5199–5209.

Lawson, N.D., Vogel, A.M., and Weinstein, B.M. (2002). sonic hedgehog and vascular endothelial growth factor act upstream of the Notch pathway during arterial endothelial differentiation. Dev. Cell *3*, 127–136.

Lenard, A., Daetwyler, S., Betz, C., Ellertsdottir, E., Belting, H.-G., Huisken, J., and Affolter, M. (2015). Endothelial Cell Self-fusion during Vascular Pruning. PLoS Biol. *13*, e1002126.

Le Guen, L., Karpanen, T., Schulte, D., Harris, N.C., Koltowska, K., Roukens, G., Bower, N.I., van Impel, A., Stacker, S.A., Achen, M.G., et al. (2014). Ccbe1 regulates Vegfc-mediated induction of Vegfr3 signaling during embryonic lymphangiogenesis. Development 1–11.

Lobov, I.B., Cheung, E., Wudali, R., Cao, J., Halasz, G., Wei, Y., Economides, A., Lin, H.C., Papadopoulos, N., Yancopoulos, G.D., et al. (2011). The Dll4/Notch pathway controls postangiogenic blood vessel remodeling and regression by modulating vasoconstriction and blood flow. Blood *117*, 6728–6737.

Lowe, D.G. (2004). Distinctive image features from scale-invariant keypoints. Int. J. Comput. Vis. *60*, 91–110.

Lucitti, J.L., Jones, E.A.V., Huang, C., Chen, J., Fraser, S.E., and Dickinson, M.E. (2007). Vascular remodeling of the mouse yolk sac requires hemodynamic force. Development *134*, 3317–3326.

Matsuoka, R.L., Marass, M., Avdesh, A., Helker, C.S., Maischein, H.-M., Grosse, A.S., Kaur, H., Lawson, N.D., Herzog, W., and Stainier, D.Y. (2016). Radial glia regulate vascular patterning around the developing spinal cord. Elife *5*.

Mehta, V., Pang, K.-L., Rozbesky, D., Nather, K., Keen, A., Lachowski, D., Kong, Y., Karia, D., Ameismeier, M., Huang, J., et al. (2020). The guidance receptor plexin D1 is a mechanosensor in endothelial cells. Nature.

Park, J.E., Chen, H.H., Winer, J., Houck, K.A., and Ferrara, N. (1994). Placenta growth factor. Potentiation of vascular endothelial growth factor bioactivity, in vitro and in vivo, and high affinity binding to Flt-1 but not to Flk-1/KDR. J. Biol. Chem. *269*, 25646–25654.

Phng, L., Potente, M., Leslie, J.D., Babbage, J., Nyqvist, D., Lobov, I., Ondr, J.K., Rao, S., Lang, R.A., Thurston, G., et al. (2009). Nrarp coordinates endothelial Notch and Wnt signaling to control vessel density in angiogenesis. Dev. Cell *16*, 70–82.

Pitulescu, M.E., Schmidt, I., Giaimo, B.D., Antoine, T., Berkenfeld, F., Ferrante, F., Park, H., Ehling, M., Biljes, D., Rocha, S.F., et al. (2017). Dll4 and Notch signalling couples sprouting angiogenesis and artery formation. Nat. Cell Biol. *19*, 915–927.

Ribatti, D., and Crivellato, E. (2012). 'Sprouting angiogenesis', a reappraisal. Dev. Biol. *372*, 157–165.

Schindelin, J., Arganda-Carreras, I., Frise, E., Kaynig, V., Longair, M., Pietzsch, T., Preibisch, S., Rueden, C., Saalfeld, S., Schmid, B., et al. (2012). Fiji: an open-source platform for biological-image analysis. Nat. Methods *9*, 676–682.

Sehnert, A.J., Huq, A., Weinstein, B.M., Walker, C., Fishman, M., Stainier, D.Y.R. (2002). Cardiac troponin T is essential in sarcomere assembly and cardiac contractility. Nat. Genet. *31*, 106–110.

Silver, A.E., and Vita, J.A. (2006). Shear-stress-mediated arterial remodeling in atherosclerosis: too much of a good thing? Circulation *113*, 2787–2789.

Simons, M., Gordon, E., and Claesson-Welsh, L. (2016). Mechanisms and regulation of endothelial VEGF receptor signalling. Nat. Rev. Mol. Cell Biol. *17*, 611–625.

Tinevez, J.-Y., Perry, N., Schindelin, J., Hoopes, G.M., Reynolds, G.D., Laplantine, E., Bednarek, S.Y., Shorte, S.L., and Eliceiri, K.W. (2017). TrackMate: An open and extensible platform for single-particle tracking. Methods *115*, 80–90.

Tzima, E., Irani-Tehrani, M., Kiosses, W.B., Dejana, E., Schultz, D.A., Engelhardt, B., Cao, G., DeLisser, H., and Schwartz, M.A. (2005). A mechanosensory complex that mediates the endothelial cell response to fluid shear stress. Nature *437*, 426–431.

Udan, R.S., Vadakkan, T.J., and Dickinson, M.E. (2013). Dynamic responses of endothelial cells to changes in blood flow during vascular remodeling of the mouse yolk sac. Development *140*, 4041–4050.

Villefranc, J., Amigo, J., Lawson, N. (2007). Gateway compatible vectors for analysis of gene function in the zebrafish. Dev. Dyn. *236*, 3077-3087.

Wild, R., Klems, A., Takamiya, M., Hayashi, Y., Strähle, U., Ando, K., Mochizuki, N., van Impel, A., Schulte-Merker, S., Krueger, J., et al. (2017). Neuronal sFlt1 and Vegfaa determine venous sprouting and spinal cord vascularization. Nat. Commun. *8*, 13991.

Wilkinson, R.N., Koudijs, M.J., Patient, R.K., Ingham, P.W., Schulte-Merker, S., Van Eeden, F.J.M. (2012). Hedgehog signaling via a calcitonin receptor-like receptor can induce arterial differentiation independently of VEGF signaling in zebrafish. Blood *120*, 477–488.

Wu, R.S., Duong, D.N., Lam, I.I., Clay, H., Coughlin, S.R., and Deo, R.C. (2018). A Rapid Method for Directed Gene Knockout for Screening in G0 Zebrafish. Dev. Cell *46*, 112-125.e4.

Zhang, Y., Xu, B., Chen, Q., Yan, Y., Du, J., and Du, X. (2018). Apoptosis of Endothelial Cells Contributes to Brain Vessel Pruning of Zebrafish During Development. Front. Mol. Neurosci. *11*, 222.

Zhou, Q., Perovic, T., Fechner, I., Edgar, L.T., Hoskins, P.R., Gerhardt, H., Krüger, T., and Bernabeu, M.O. (2020). Association between erythrocyte dynamics and vessel remodelling in developmental vascular networks (bioRxiv).

Zygmunt, T., Gay, C.M., Blondelle, J., Singh, M.K., Flaherty, K.M., Means, P.C., Herwig, L., Krudewig, A., Belting, H., Affolter, M., et al. (2011). Semaphorin-PlexinD1 Signaling Limits Angiogenic Potential via the VEGF Decoy Receptor sFlt1. Dev. Cell *21*, 301–314.

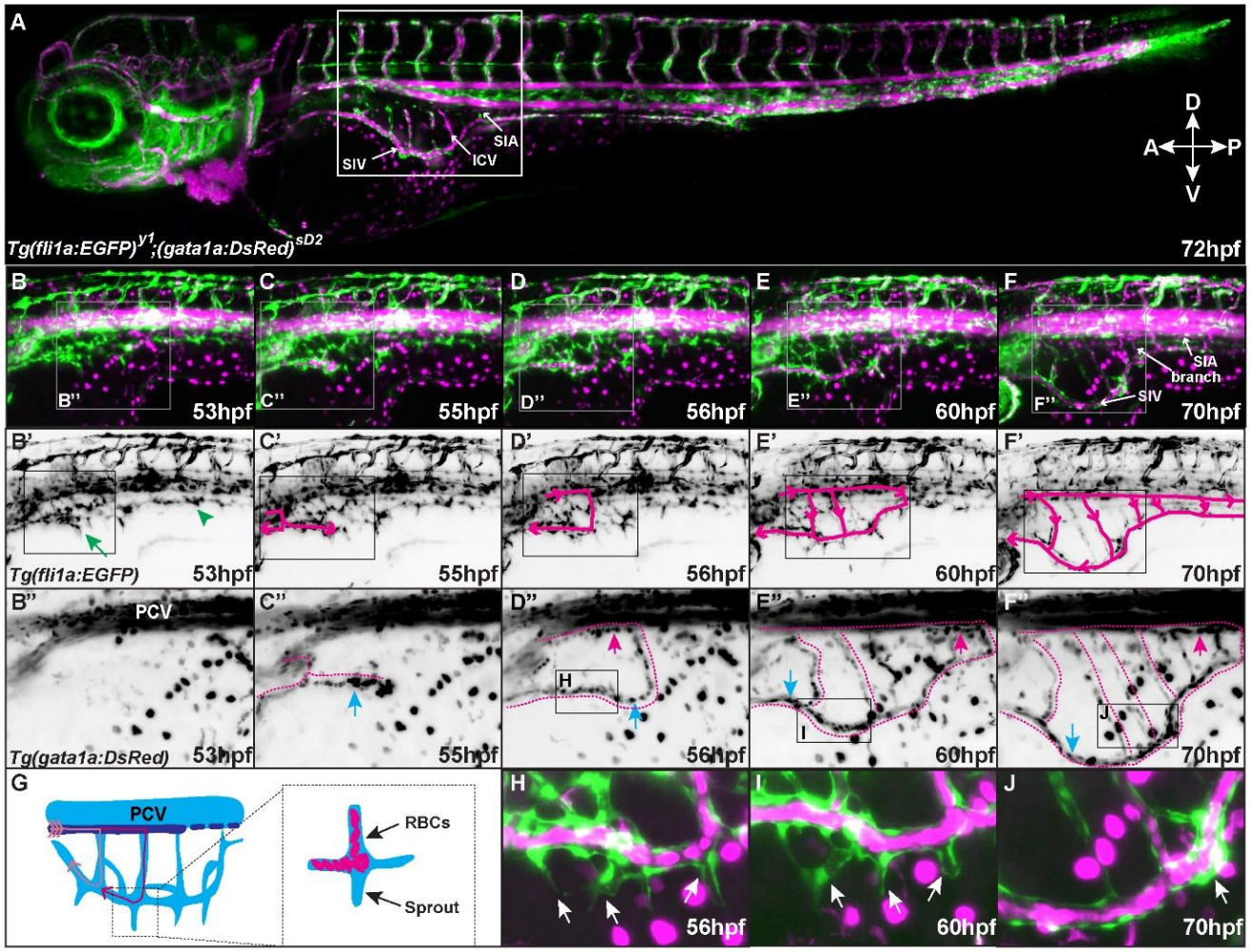

Figure 1 SIVP perfusion is coincident with leading sprout regression

(**A-F**) Representative images taken from a time-lapse (Supplementary Movie 1) between 53-70hpf showing perfusion of the sub-intestinal venous plexus (SIVP). *Tg(fli1a:EGFP)*^{y1} was used to label endothelial cells (green) and *Tg(gata1a:DsRed)*^{sD2} labels erythrocytes (magenta). Region highlighted in A is displayed in B-F, and region highlighted in B-F is enlarged in B'- F'. Region highlighted in B'-F' is enlarged in B''-F'' and displays the path of circulating erythrocytes. Circulation enters the anterior SIVP between 53hpf (**B-B''**) and 55hpf (**C-C''**) and perfuses the SIV from anterior to posterior as it develops (**D-F''**). Blood enters the SIVP from the supraintestinal artery (SIA) (**D'-F''**, magenta arrows) an extension of the upstream anterior mesenteric artery, through the SIVP branches, drains into the SIV (**C''-F''**, blue arrows) and exits the SIV via the hepatic portal vein (HPV). **G**) Schematic representation of SIVP perfusion. **H-J**) Leading sprouts are observed to regress and undergo anastomosis in the presence of blood flow (arrows). ICV, inter-connecting vessel; PCV, posterior cardinal vein; RBC, red blood cells; SIA, supra-intestinal artery; SIV, sub-intestinal vein.

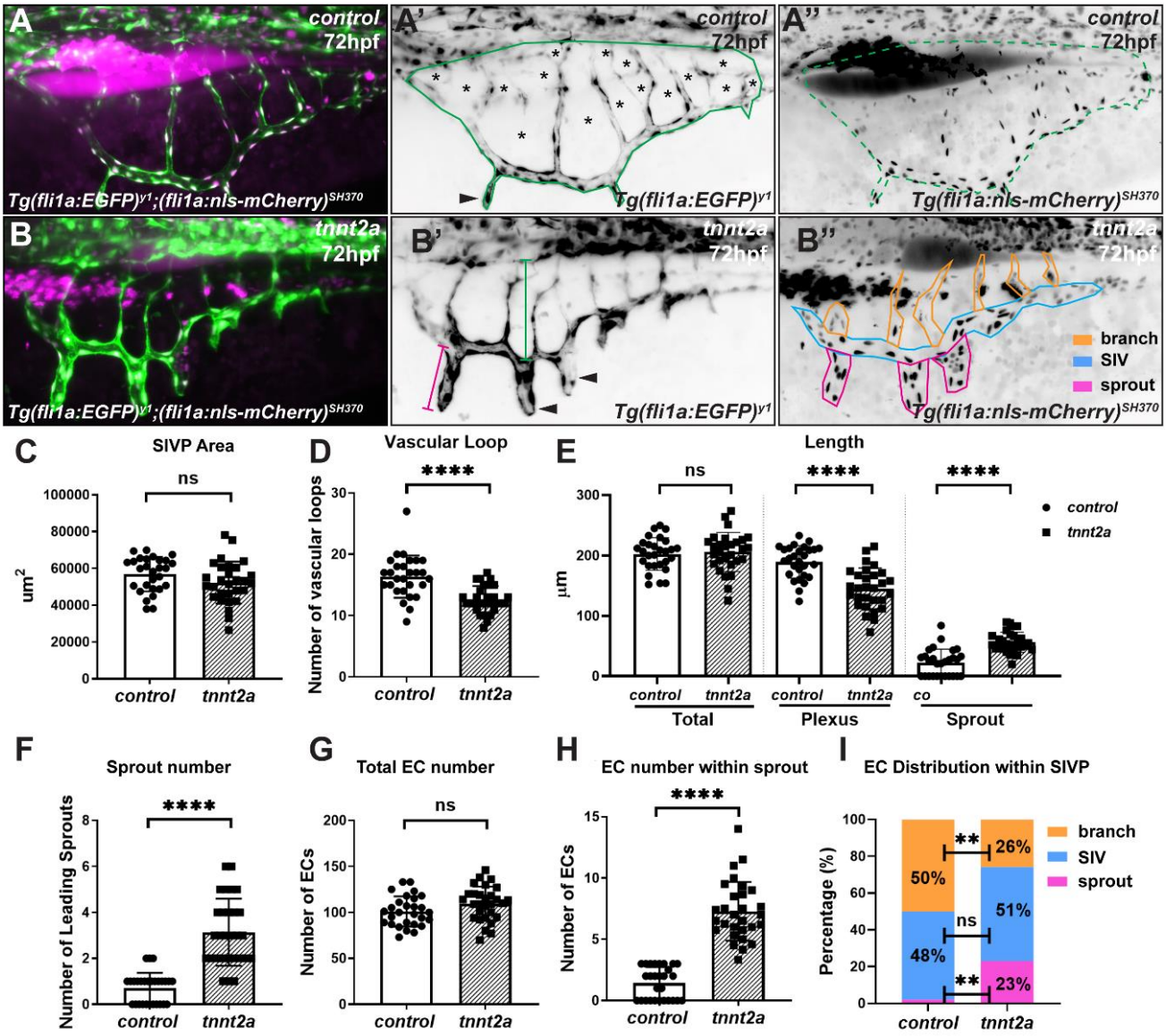

Figure 2 Blood flow controls morphology and endothelial cell distribution of the SIVP

A, **B**) Comparison of SIVP morphology at 72hpf in the presence (control morphants, **A**) or absence of blood flow (*tnnt2a* morphants). **B**) No significant difference in plexus area (highlighted in green in **A'**, **A''**) was observed in the presence or absence of blood flow (**C**). Embryos without blood flow displayed fewer vascular loops (**A'**, asterisks, **D**). Total length of the SIVP plexus was not altered in the presence or absence of blood flow (**B**', green line, **E**), however *tnnt2a* morphant embryos displayed reduced length of the SIVP basket (**B'**, blue line, **E**) and increased sprout length (**B'**, magenta line, **E**). The number of leading sprouts (**A'**, **B'** arrowheads) were increased in *tnnt2a* morphant embryos (**B''**, highlighted in magenta, **F**). The total number of ECs in the SIV was not altered by the flow status of the plexus (**G**), however, leading sprouts contained increased numbers of ECs in *tnnt2a* morphant embryos (**B''**, highlighted in magenta, **H**). In the absence of blood flow, SIV branches contained fewer ECs (**B''**, highlighted in orange, **I**). Unpaired *t*-test, ****$p \leq 0.0001$, ns; $p \geq 0.05$, control embryos, n=28; *tnnt2a* embryos, n=29.

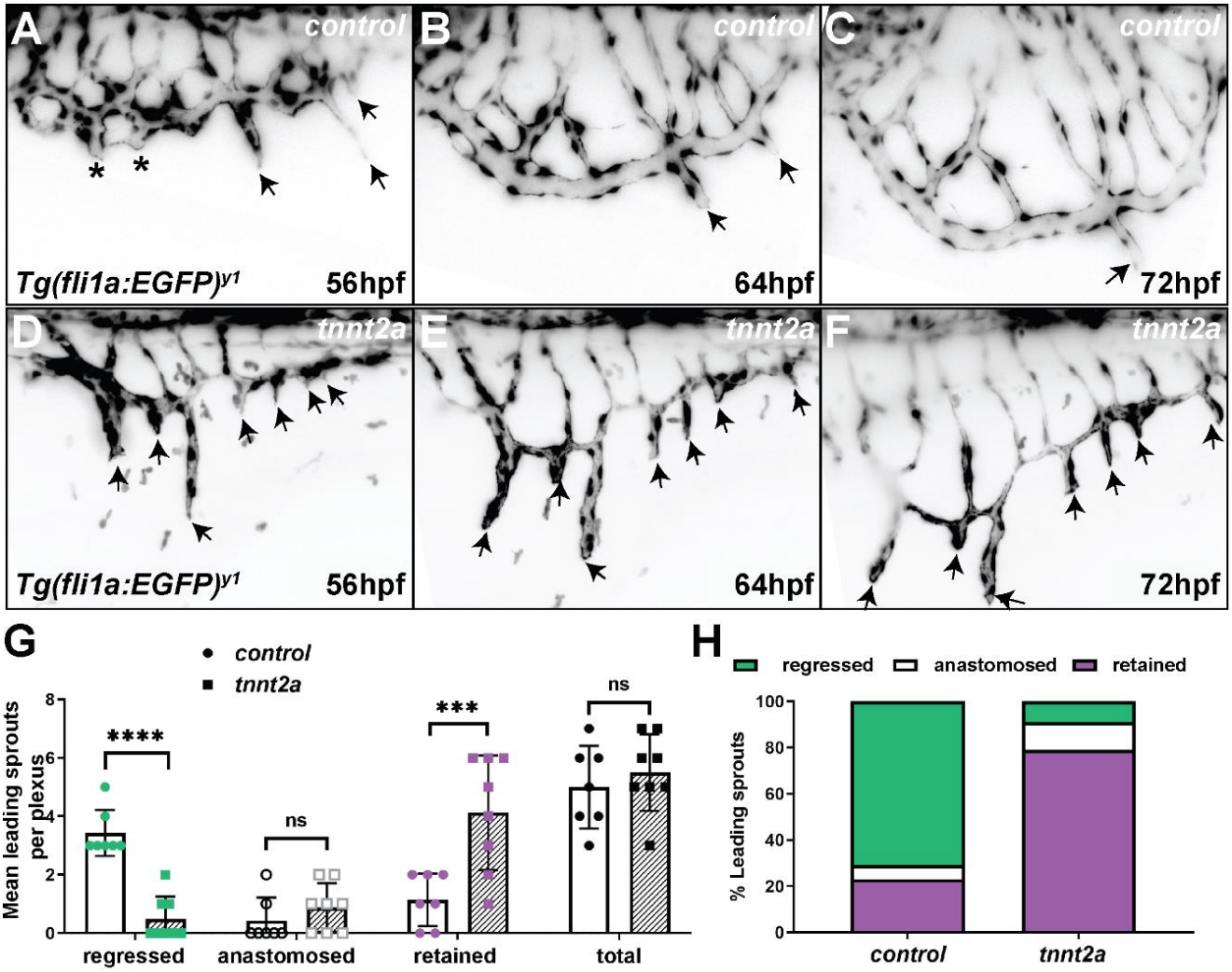

Figure 3 Blood flow promotes regression of SIVP leading sprouts

A-F) SIVP development 56-72hpf in the presence and absence of flow. Still images taken from time lapse movies (Supplementary Movie 3). **A**) In control animals, before blood flow enters the plexus, some angiogenic sprouts from the primary SIV anastomose (asterisks) to form vascular loops, while others lead at the migration front (arrows). **B**, **C**) In controls, leading sprouts regressed following the onset of blood flow and sprout ECs became incorporated into the SIV (arrows). **D-F**) In the absence of flow, leading sprouts failed to regress (**D-F**, arrows). **G, H**) Leading sprout regression was significantly reduced in *tnnt2a* morphant embryos and thus, the number of sprouts present at 72hpf were increased in comparison to controls. Unpaired *t*-test **** $p \leq 0.0001$; *** $p \leq 0.001$; ns $p \geq 0.05$; control morphants n=8; *tnnt2a* morphants n=7.

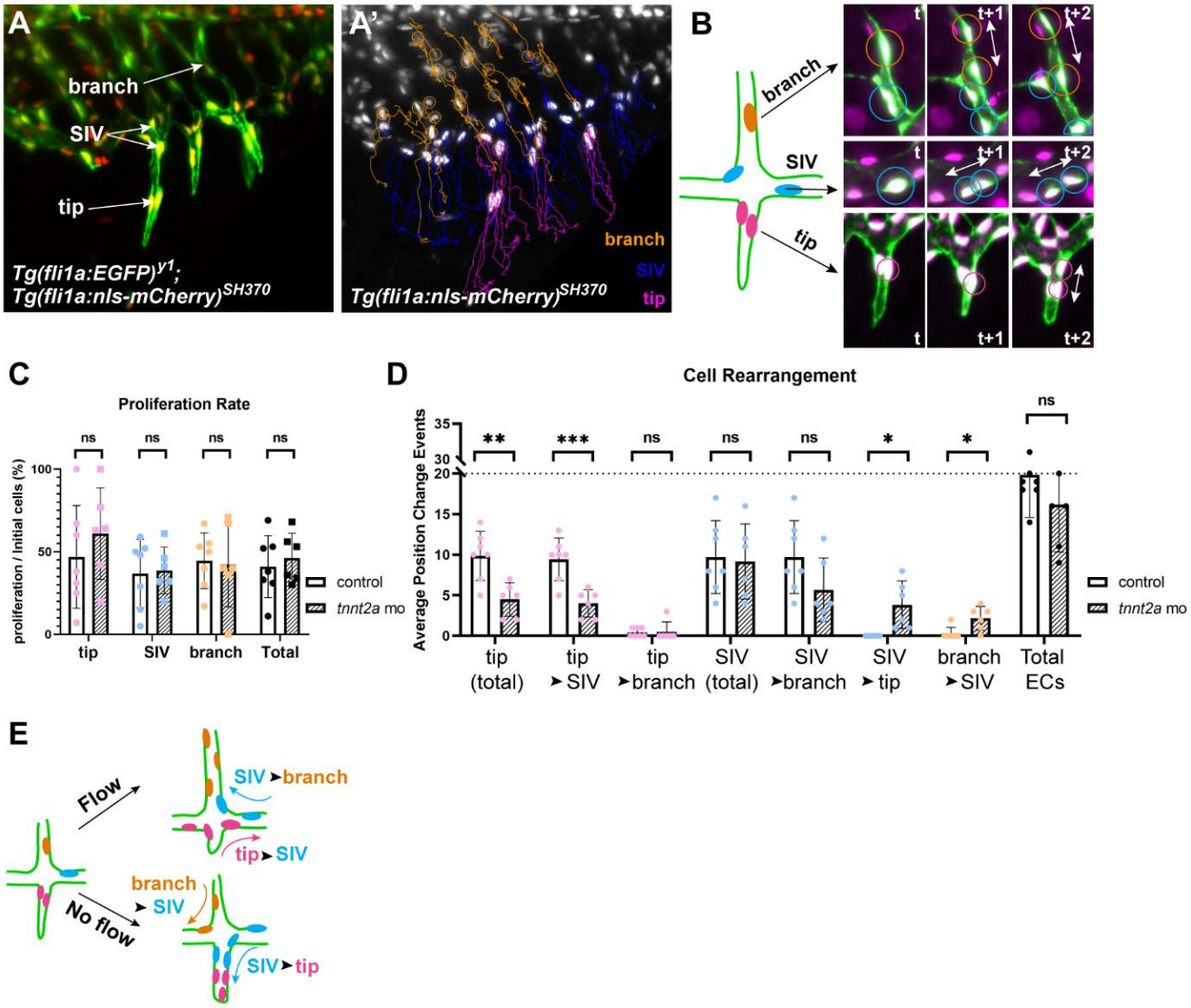

Figure 4 Blood flow coordinates EC migration but not proliferation within the developing SIVP

A-B) ECs in the SIVP were divided into three groups depending upon their initial position at 56hpf. SIVP branch cells (orange) within branches, SIV cells (magenta) within the ventral SIV (blue) and tip cells within leading sprouts (magenta). Examples of EC proliferation in subsequent timepoints are highlighted (**B**). The direction of cell division is parallel to the long axis of the vessel (**B**). **C**) EC proliferation rate (cell division events/initial number of ECs) did not differ in total or between groups in the presence or absence of flow. **D**) There was a substantial reduction in tip cell contribution to SIV in *tnnt2a* morphants, indicating that flow is required for dorsal tip cell rearrangement. In addition, there was an increase in ventral migration of SIV ECs into leading sprouts in the absence of flow. Most branch cells remained in the branches under flow, however, more branch ECs migrated ventrally to contribute to the SIV without blood flow. **E**) Schematic representation of differing EC migration in the presence and absence of blood flow. Unpaired *t*-test ***$p \leq 0.001$; **$p \leq 0.01$; *$p < 0.05$; ns $p \geq 0.05$, control morphants n=7; *tnnt2a* morphants n=6.

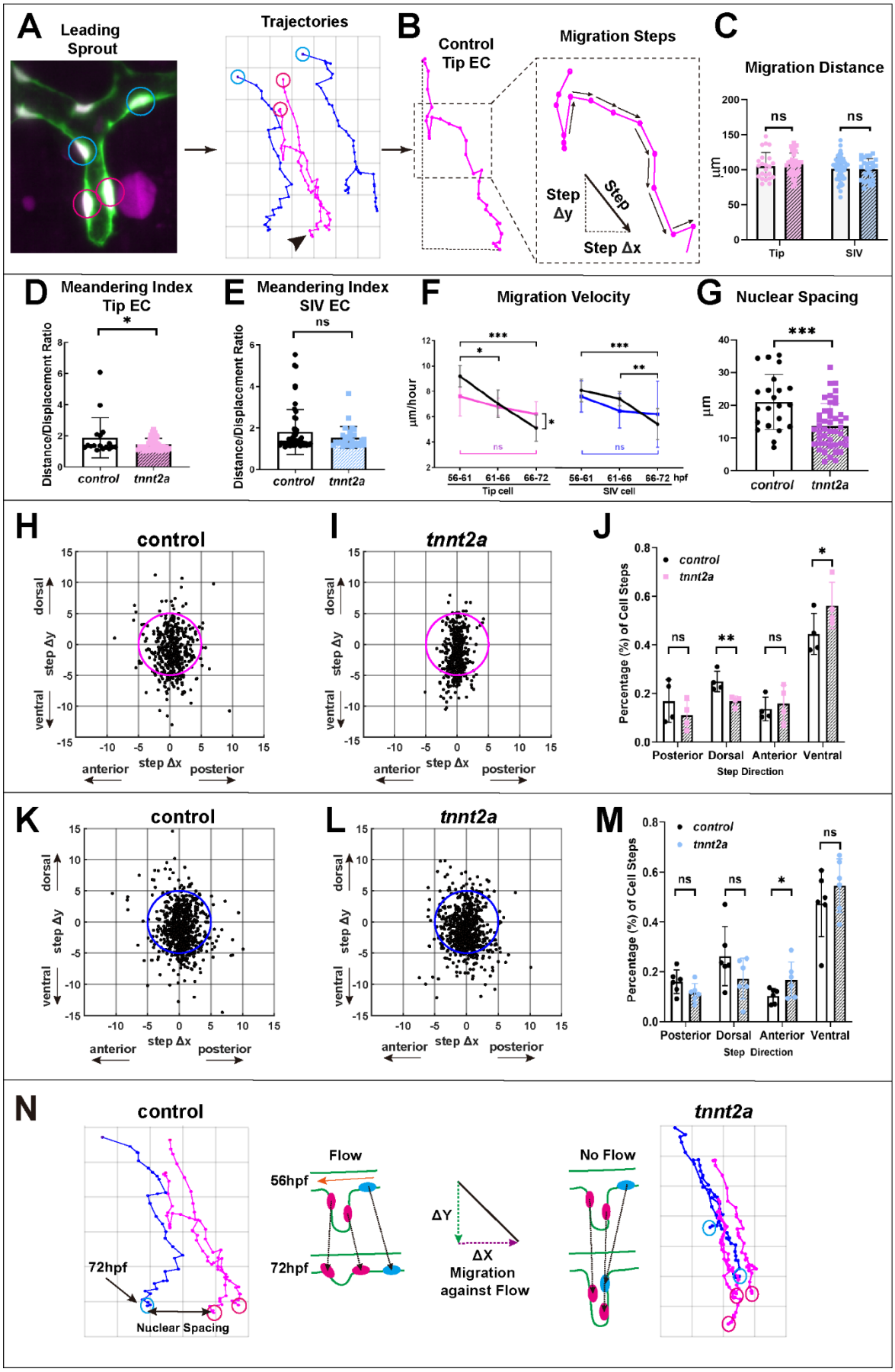

Figure 5 Blood flow controls EC migration direction during leading sprout regression

A) Examples of ECs within the SIV (blue) or tip cells (magenta) tracked in proximity to leading sprout and example migration trajectories. **B**) Migration 'steps' are defined as the movement of ECs between two consecutive time points (arrows). **C**) Migration distance (the sum of step displacements) of SIV ECs or tip cells was unaffected by flow status of SIVP. (**C-E**) Each dot represents a migration track of a single EC. control, n=79 tracks from 5 embryos; *tnnt2a*, n=64 tracks from 5 embryos. Tip cells: control, n=23 tracks, *tnnt2a*, n=37 tracks; SIV cells, control, n=56 tracks, *tnnt2a*, n=27 tracks; Unpaired *t*-test **D, E**) Meandering index was significantly reduced in tip cells in *tnnt2a* morphants (**D**) but was not significantly different in SIV ECs (**E**). **F**) Migration velocity of tip or SIV cells gradually reduced in the presence of flow (black lines) but was not significantly altered in *tnnt2a* morphants (coloured lines). Average speed of every step of tip cells or SIV cells from 6 control or *tnnt2a* embryos. Unpaired *t*-test. **G**) Nuclear spacing was significantly reduced in *tnnt2a* morphants indicating increased EC crowding within the SIVP. Control, n=22 from 6 embryos; *tnnt2a*, n=46 from 6 embryos. Unpaired *t*-test **H**-**J**) Scatter plots displaying coordinates of tip cell migration steps. The magenta circle in each plot (5µm radius) is outlined as a reference for coordinate distribution. Migration steps show increased alignment along Y-axis in *tnnt2a* mutants (**I**) in comparison to controls (**H**) and tip cells display significant reduction in dorsal and increase in ventral migration in the absence of blood flow (**J**). control, n=383 steps from 4 embryos; *tnnt2a*, n=860 steps from 4 embryos. **K-M**) Scatter plots displaying coordinates of SIV EC migration steps indicate increased migration steps in quadrant III in *tnnt2a* morphants (**L**) indicating anterior migration bias in the absence of blood flow (**M**). control, n=1313 steps from 6 embryos; *tnnt2a*, n=744 steps from 6 embryos. **N**) Schematic representation of EC migration within the SIVP during sprout regression. In the presence of flow, SIV cells migrate laterally to accommodate dorsally migrating tip cells as leading sprouts regress. In the absence of flow, SIV ECs migrate more anteriorly, and tip cells migrate ventrally leading to elongated sprouts and regression failure. **** $p \leqslant 0.0001$; *** $p \leqslant 0.001$; ** $p \leqslant 0.01$; * $p < 0.05$; ns $p \geq 0.05$.

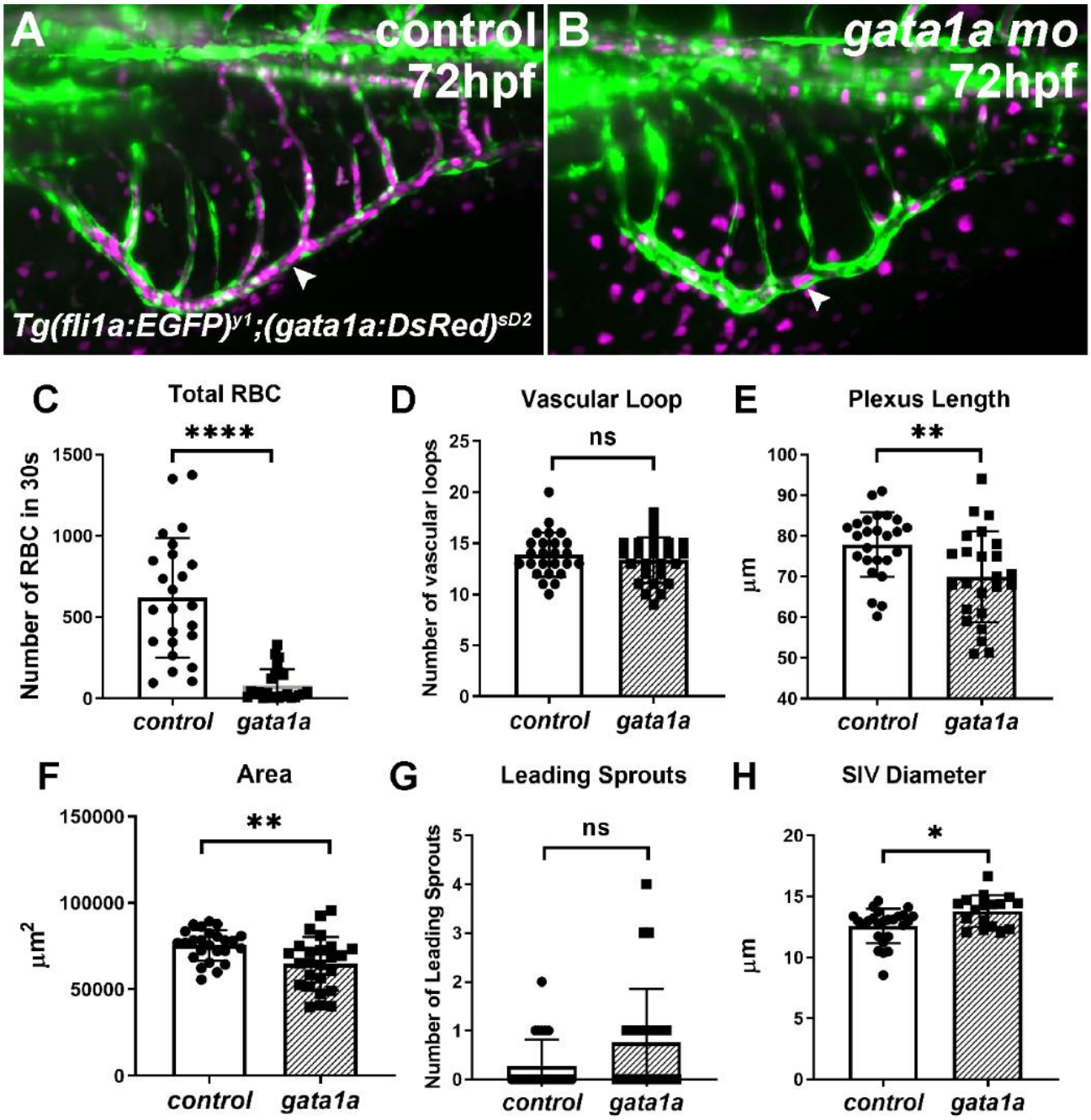

Figure 6 Leading sprout regression occurs under conditions of reduced blood flow

Leading sprouts undergo normal regression in *gata1a* morphants (**A**) in comparison to controls (**B**) despite a substantial reduction of circulating erythrocytes in *gata1a* morphants (**C**). Frequency of vascular loops did not differ between *gata1a* morphants and controls (**D**), but plexus length (**E**) and area (**F**) was reduced in *gata1a* morphants. Frequency of leading sprouts was not significantly altered in *gata1a* morphants (**G**), but SIVP diameter was increased in these embryos (**H,** arrowhead). Unpaired *t*-test, **** $p \leqslant 0.0001$; ** $p \leqslant 0.01$; * $p < 0.05$; ns $p \geq 0.05$; control morphants n=24, *gata1a* morphants n=24, 3 replicates.

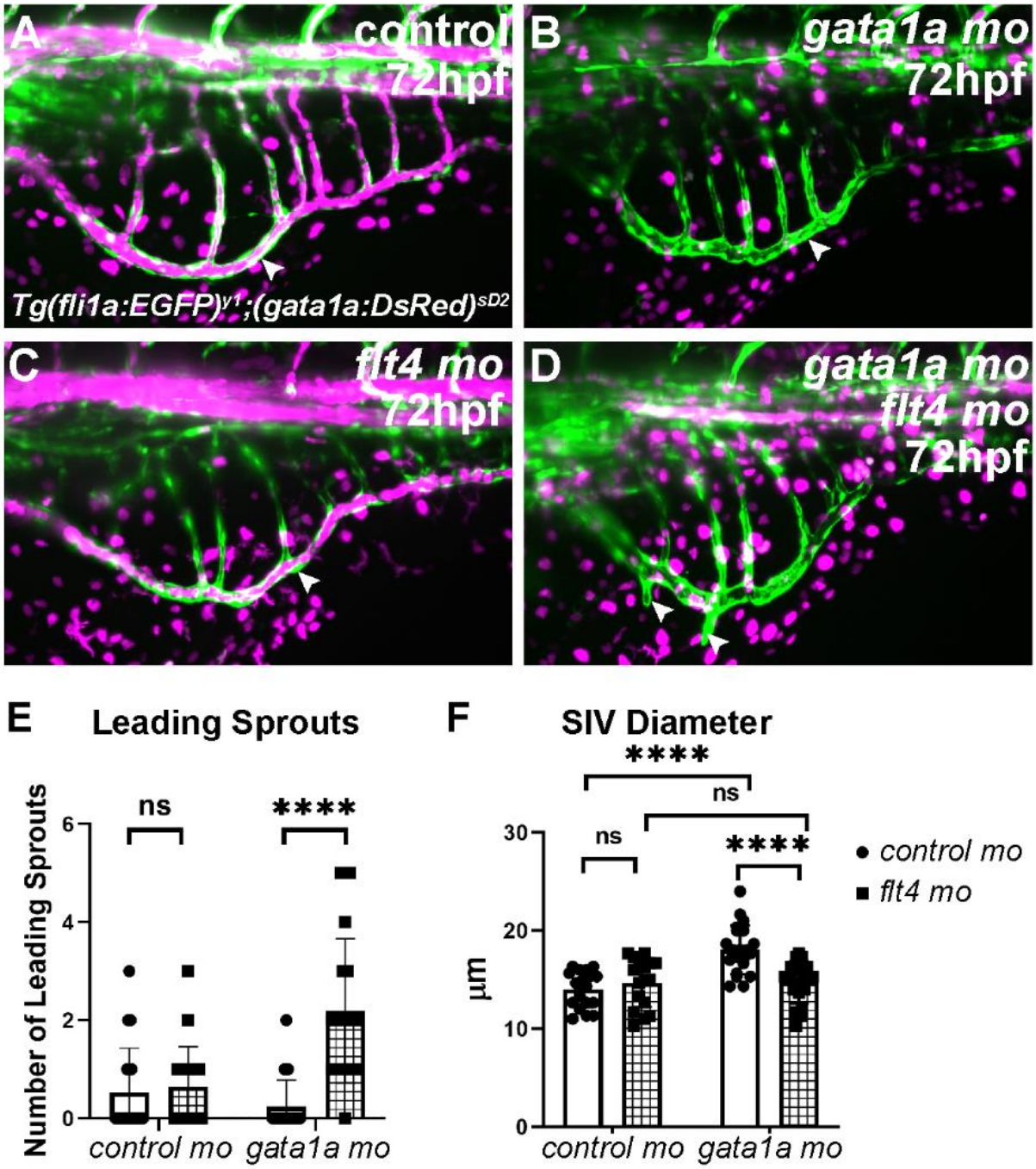

Figure 7 Leading sprout regression under low blood flow conditions is dependent on *flt4*

In comparison to controls (**A**), *gata1a* morphants displayed reduced circulating erythrocytes within the SIVP without inhibiting leading sprout regression (**B**, arrows). Leading sprout regression was unaltered by *flt4* knockdown under normal flow conditions (**C**) but *flt4* knockdown inhibited sprout regression under low flow conditions (**D**, arrows). The frequency of leading sprouts was significantly increased in *flt4*/*gata1a* double morphants compared to either *flt4*, *gata1a* or control single morphants (**E**). SIV diameter was enlarged under low flow conditions in *gata1a* morphants, but this was reduced following *flt4* knockdown under low flow conditions (**F**). Two-way ANOVA, **** $p \leqslant 0.0001$; *** $p \leqslant 0.001$; ** $p \leqslant 0.01$; ns $p \geq 0.05$. control morphants n=19; *flt4* morphants n=19; *gata1a* morphants n=21; *flt4; gata1a* morphants n=21, 3 replicates.

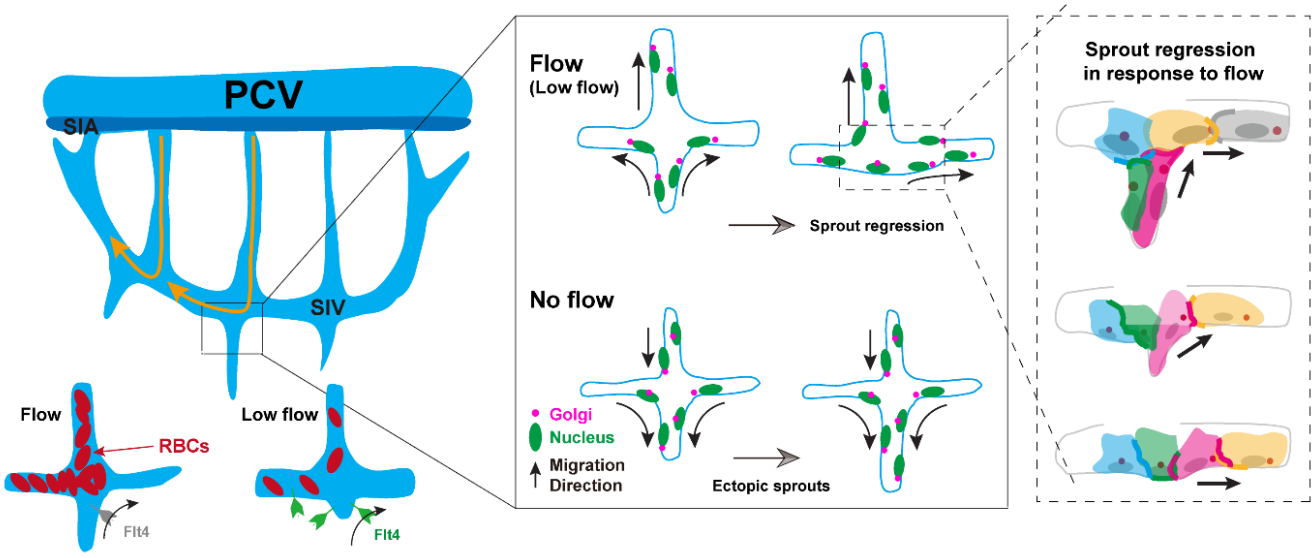

Figure 8 Cellular mechanisms of flow-mediated sprout regression

Schematic illustrations depicting the cellular behaviours during SIVP sprout regression in the presence and absence of flow. Blood flow promotes EC Golgi polarisation, dorsal and lateral EC migration and leads to sprout regression via Flt4 under low blood flow conditions. Illustrations highlighted with dashed lines depict co-ordination of EC migration during sprout regression in response to flow. ECs (in grey and yellow) at the luminal surface migrate laterally against flow and ECs (in green and pink) in the regressing sprout are pulled or use their neighbouring cells as migratory substrates via EC junctions (thickened lines), followed by EC rearrangements which lead to sprout regression. Abbreviations; PCV posterior cardinal vein; RBCs, red blood cells; SIV; sub-intestinal vein; SIA, supra-intestinal artery